Available online at www.sciencedirect.com

ScienceDirect

Procedia Manufacturing 47 (2020) 1345–1352

Procedia MANUFACTURING

www.elsevier.com/locate/procedia

23rd International Conference on Material Forming (ESAFORM 2020)

Extension of the Conventional Press Hardening Process by Local Material Influence to Improve Joining Ability

Bernd-Arno Behrens[a], Sven Jüttner[b], Kai Brunotte[a], Fahrettin Özkaya[a], Maximilian Wohner[b] and Eugen Stockburger[a,*]

[a]*Institut für Umformtechnik und Umformmaschinen, Leibniz Universität Hannover, An der Universität 2, 30823 Garbsen, Germany*
[b]*Institut für Werkstoff- und Fügetechnik, Otto-von-Guericke-Universität Magdeburg, Universitätsplatz 2, 39106 Magdeburg, Germany*

* Corresponding author. Tel.: +49-511-762-3913; fax: +49-511-762-3007. *E-mail address:* stockburger@ifum.uni-hannover.de

Abstract

Press hardened structural components are a key factor in lightweight car design and thus in reducing vehicle mass while increasing crash safety. The use of quenched 22MnB5 (Usibor 1500) has been established in hot sheet forming for the production of safety-relevant car body components. In order to expand the field of application for press-hardened components, a process-reliable joining technique is essential. Ultra-high-strength components can be joined with other parts in car bodies using the resistance spot welding process. Here, challenges like uneven welding lens formations with an incorrect connection in multi-sheet joints arise. Mechanical joining processes, for example self-pierce riveting, can only be used to a limited extent due to the high hardness of the hardened parts. For this purpose, an annealing treatment is often carried out in order to reduce the strength of the material after press hardening. Another possibility to create softened areas is the introduction of local deformation in the austenitic material. The phase areas in the continuous cooling transformation diagram are shifted to shorter cooling times, which enables the development of deformation-induced ferrite. The local thinning and softening improves joinability by means of mechanical and thermal joining processes but increases the forming force. Therefore, in this study the process of hot forming and local deformation is first pre-estimated using numerical simulation. The required force for the deformation and an optimal positioning, as well as the possible number of deformation punches, are investigated. Furthermore, the first experimental results of the feasibility of locally thinned and softened sheets are presented. In addition, joining tests by resistance spot welding and self-pierce riveting are carried out on the generated specimen to illustrate the practical effectiveness of the local thinning and the use of deformation-induced ferrite for critical joints.

Keywords: Press hardening; deformation-induced ferrite; FE-simulation; self-pierce riveting; resistance spot welding

1. Introduction

1.1. Process route of press hardening

In the automotive industry, high demands are placed on lighter body components with high rigidity and crash safety. To meet the requirements, steel materials with high strengths and reduced thicknesses are used [1]. The low forming capacity and high strength of these materials leads to a challenge for production technology, in order to create complex body components. In the production of structural chassis parts, such as A-, B-pillars and roof frames, press hardening has been established. Press hardening is a manufacturing process, which allows to form an ultra-high strength steel into a complex geometry with low forming forces. Manganese-boron steels are mostly used as materials. During press hardening, the material is formed and quenched which results in a martensitic microstructure with increased tensile strengths up to 1,600 MPa and elongations at the break between 5 % and 7 % [2]. The advantages are a high hardness of the components, a high dimensional as well as shape accuracy, low elastic spring back and low residual stresses.

2351-9789
10.1016/j.promfg.2020.04.258

There are two process routes for press hardening of car chassis components: direct and indirect press hardening. In the direct route, a blank is heated up to austenitisation temperature, dwells a certain time in the oven and is subsequently transferred to the forming tool. Indirect press hardening additionally involves a pre-forming process at room temperature to produce components of higher complexity. In this process route, the main forming operation often takes place during preforming [3].

1.2. Joining of press hardened steels

Due to the advancing e-mobility, the sheet thicknesses of press hardened steel are continually increasing [4]. This can be explained by the use of battery cells, which require higher strength in the area of the floor assembly [5]. In order to achieve a weight reduction of the body in white (BIW), new lightweight construction concepts using different materials, thicknesses and coatings are developed [6]. This results in new challenges for joining technology, such as resistance spot welding of asymmetrical multi-sheet stack-up from press hardened components and other vehicle components.

Multi-sheet joints created by resistance spot welding can result in a vertical shifting of the nugget, which is accompanied by the insufficient joining of the thin outer sheet. Similarly, the joining of press hardened steels by self-pierce riveting is limited and has only been possible in small process windows because of the high material hardness. Both problems are shown in Fig. 1 (a).

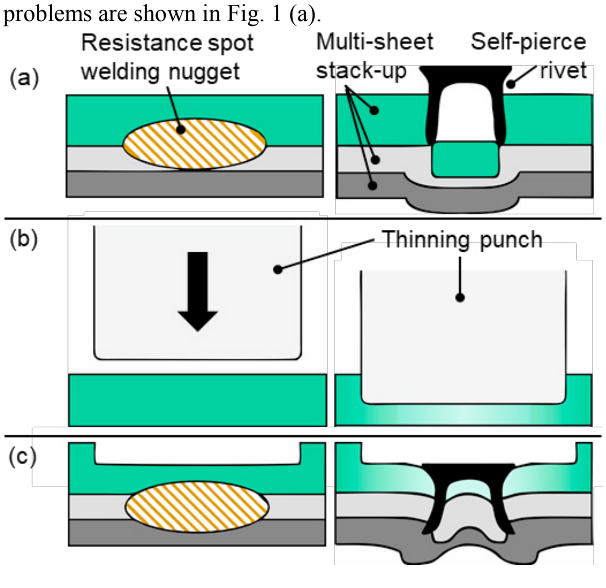

Fig. 1. (a) Initial conditions for resistance spot welding (left) and self-pierce riveting (right); (b) creating the local thinning and softening; (c) joining with adapted sheet thickness combination.

The phenomenon regarding the shifted nugget can occur if a critical sheet thickness ratio of 1:3 of the joining partners is exceeded [7]. Furthermore, the selected joining partners and the materials increase this effect. In general press hardened steel (22MnB5+AS150) has a higher bulk and contact resistance than other steel grades. The result is a lower nugget penetration depth, whereby the more conductive material is not or only insufficiently attached. A large number of publications deal with the compensation of this joining problem [8, 9, 10]. These investigations focus primarily on the modification of the welding electrodes as well as the welding parameters. In contrast, only a few adjustments were made to the welding work piece itself [10]. Using specially adapted self-piercing riveting (RIVSET® HDX) and tools, it is possible to join steels with a strength of up to 1.600 MPa and a maximum sheet thickness of 1.7 mm by self-pierce riveting [11]. In addition to the given process limits, the formation of pockets in the flange area can occur, which in combination with adhesive can lead to insufficient adhesive bonding. Therefore the high strength in press hardened components must be reduced partially and thus be able to use more cost-effective self-piercing riveting. The subsequent local reheating of press hardened steel is one of these possibilities. Partial tempering of the material represents an additional process step and can be performed, for example, using a laser, or by inductive or conductive heating [12].

1.3. Deformation-induced ferrite

Press hardened components with locally varying material properties can be produced by different processes. The austenitisation and quenching process can be changed or an additional annealing step can be performed after hardening. Possibilities to influence resulting mechanical properties during the heating process by tailored tempering were investigated in [13]. Certain areas of the blank were covered with masks during heating to prevent austenitisation. During the combined forming and quenching process, it is also possible to influence the microstructure transformation by targeted heating of the tool. Banik et al. observed that tool temperatures between 300 °C and 550 °C could be used to adjust various property combinations of strength and ductility [14]. However, this leads to a gradient of mechanical properties in the component at the transition areas between the cooled and heated tool areas. In [15], a method is investigated by suppressing the hardening during press hardening selectively by adapted tool technology. Heated pins are used in the tool for partial quenching, which prevents the transformation of austenite into martensite in the component during die hardening. An additional option for modifying the material properties after the forming process is annealing. Zimmermann et al. have determined a fracture elongation of 28.4 % on previously completely hardened specimens by annealing at temperatures up to 800 °C [16]. Spot annealing by laser radiation was investigated [17]. In [18] a softening of the hardened components was carried out in a subsequent process step using local annealing processes such as conductive, inductive and laser methods.

Another possibility to change the microstructure transformation behaviour of steels is a thermo-mechanical treatment. Due to a deformation of the austenitic material, the phase areas in the CCT-diagram are shifted to lower times. In order to achieve a completely martensitic microstructure in 22MnB5 for a deformation of 10 %, a critical cooling rate of 50 °C/s instead of 27 °C/s is required [19]. Furthermore, the formation of ferrite above the actual ferrite start temperature is possible. Ferrite formed this way is called deformation-induced ferrite (DIF). By forming the austenite, some of the deformation energy is stored in it. This lowers the nucleation energy and leads to the formation of DIF. Compared to conventional ferrite, DIF is not created by grain growth, but primarily by nucleation. The reduction of the nucleation energy favours the formation of ferrite [20]. The formation of DIF is influenced by various parameters such as the forming temperature, the deformation degree and the cooling rate. As the forming temperature decreases, the formation of DIF increases. This is due to the increase in flow stress with decreasing temperature. Therefore, more energy to form the material is required, increasing the deformation energy stored in the austenite. Min et al. determined the formation of deformation-induced ferrite at an austenitisation temperature of 900 °C and a cooling rate of 30 °C/s between forming temperatures of 600 °C and 800 °C [21]. The results reveal that the deformation energy stored in the austenite increases with decreasing forming temperature. The lowest ferrite content was measured at forming temperatures of 800 °C and no DIF was formed at 900 °C. Regarding the deformation degree, the formation of DIF increases with higher deformation. This is due to the increase in dislocations in the microstructure and thus to an increase in the stored deformation energy [22].

The effect of deformation-induced ferrite creation will be used in this research to locally deform the sheet material prior to martensite formation in order to achieve softer areas, as shown in Fig. 1 (b). The deformation is carried out directly after hot deep drawing and before die quenching. Therefore, it does not represent an additional process, because it is performed within the press hardening process. The local thinning improves the resistance spot welding and the local softening by DIF enhances the self-pierce riveting, as shown in Fig. 1 (c). To investigate resulting process parameters of certain steps of the process route, a numerical model of the process is created. Within the research, values such as maximum temperatures, plastic strains and forming forces are evaluated regarding the creation of DIF. Further, first experimental tests to create local thinning and softening are carried out and analysed based on the numerical results. As a basis for the joining investigations, the initial conditions, i.e. press hardened steels without local deformation, are examined. For resistance spot welding, a material combination is used, which shows an insufficient connection of the outer sheet. For self-pierce riveting a material combination is used, which can only be joined using special self-piercing rivets. Subsequently, the influence of material thinning and the change in material strength of the respective joint will be investigated.

2. Methodology

2.1. Material characterisation and FE-simulation model

The considered press hardening process relates to chapter 1.1, but is reduced to the transfer from the furnace to the forming press and the hot deep drawing. In addition, the process is extended by hot thinning after hot deep drawing. The aim of the numerical investigation is to estimate, if the resulting temperature in the flange after hot deep drawing is within the temperature range, in which DIF can be created. Furthermore, the optimal placement of thinning punches in the flange of the demonstrator is analysed. In addition, a possible number of thinning punches is evaluated, since the forming force may exceed the maximal forming force of the forming machine.

First, a two-stage simulation model of the press hardening process, consisting of a transfer process and hot deep drawing, has been developed. The press hardening process is modelled numerically using Simufact.Forming 15. The fully austenitic sheet blank with a temperature of 930 °C is transferred from the furnace. The time for the transfer was estimated with 7 s and was simulated as a cooling by convection and thermal radiation. The 3D simulation model for the hot deep drawing with the associated boundary conditions are shown in Fig. 2.

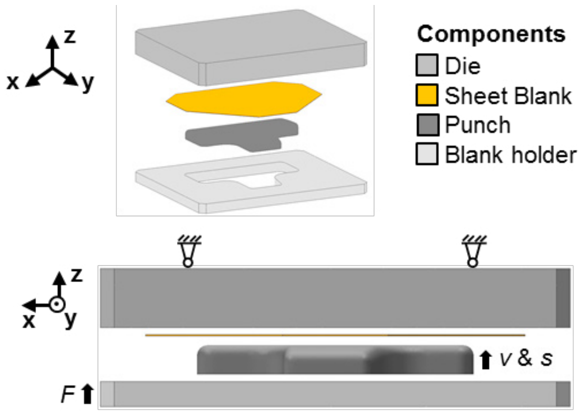

Fig. 2. Simulation model of the demonstrator for hot deep drawing with punch speed *v*, holding force *F* and punch displacement *s*.

The demonstrator's geometry is in accordance with the lower part of a B-pillar. The model includes the fixed die, the 1.5 mm thick sheet blank, the movable blank holder and the forming punch. The punch moves with the punch speed *v* of 30 mm/s and the punch displacement *s* of 30 mm. The holding force *F* applied to the blank holder corresponds to 150 kN and is modelled by a spring force. The temperature of the tools is considered to be 150 °C as it appears in the industrial case. For modelling the contact, the Coulomb friction law is used and a friction coefficient of 0.35 is selected based on the Simufact Forming 15.0 database. A pressure dependent heat transfer coefficient according to [23] is used. The specimen is modelled as elastic-plastic and the tools as rigid bodies with thermal conduction. Solid-shell elements based on hexahedron shape with five shell layers over the sheet thickness with an edge length of 4 mm are used to discretise the specimen's geometry. 210 GPa is selected for the elastic modulus of the specimen material 22MnB5, 0.3 for the Poisson's ratio and 7.8 kg/dm³ for the density. The flow behaviour of the specimen material is described with the von Mises yield criterion. The hardening behaviour at process-relevant temperatures is characterised with tensile tests at a forming simulator Gleeble 3800-GTC. Therefore, the specimens are heat treated in accordance with the process route and subsequently tested at evaluated temperatures with a strain rate of 0.2 1/s until fracture. The material data for the tool steel 1.2367 is taken from Simufact material database. An implicit solver is used for the calculation. Second, the simulation model has been extended by a next process step for the generation of a local thinning in the flange. The optimal placement of the thinning punches was estimated based on the results of the hot deep drawing simulation. For this purpose, the blank holder was designed with holes drilled in the appropriate places. A refinement box is placed in those areas creating a local element edge length of 0.5 mm in order to be able to simulate the thinning process correctly. The thinning punch is a basic cylinder. Its diameter d_P was set to 20 mm and the forming depth t_P, which corresponds to the depth the punch enters the flange, to 0.5 mm. The forming speed is equivalent to the punch speed v of 30 mm/s.

2.2. Test setup for local thinning and local softening experiments

The experiments for the creation of DIF are carried out on the Weingarten impact bonding press type PSR 160. The forming press was chosen based on the numerical findings of the resulting forming force of the local thinning. For this purpose, heatable tools with different geometries of the deformation element are used. The lower tool contains a deformation element, whereas the upper tool is plane. For the different tools the hardened tool steel 1.2367 was used and for the tests the sheet material 22MnB5 with a sheet thickness of 1.5 mm. In the first step, the specimen was heated up to a temperature of 930 °C for 6 min in a furnace and thus completely austenitic. In order to avoid a rapid temperature loss when placing the sheet material on the tool, spring pins were integrated into the lower tool. The heated tools reduce the heat loss from the sheet material. The lower tools were heated in the furnace up to a temperature of 550 °C, while the upper tool was fixed and therefore heated with heating cartridges up to a maximal temperature of 280 °C. Fig. 3 shows the experimental setup for the local thinning to generate DIF.

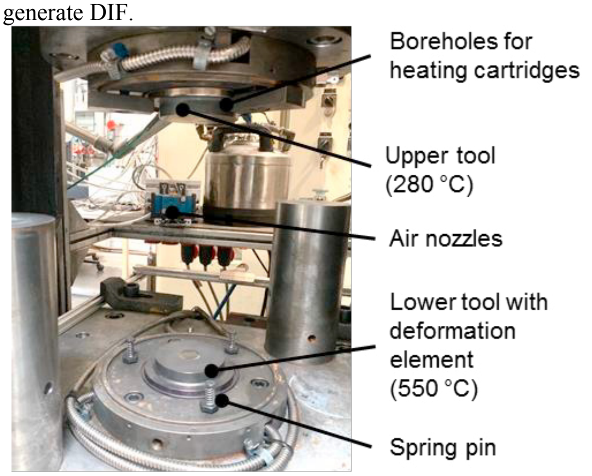

Fig. 3. Experimental setup for the introduction of local thinning and softening.

To ensure the temperature for forming and to set a defined cooling rate, a thermocouple was spot welded on the centre of the specimen. The thinning experiments were carried out following the simulation results to be as close as possible to the actual forming process and to be in the range of DIF formation. An air cooling system is mounted on the press, which moves over the sheet material after the forming operation. It cools down the deformed blank specimens using compressed air with a moderate cooling rate in the range of 30 K/s to 50 K/s to be in the process window of DIF creation.

2.3. Selection of critical joints in the initial condition

In order to define the requirements for the joining conditions of sheet thinning and material influence, analogy tests were carried out. The riveting tests were performed using the following analogy method. Instead of the thinning created during press hardening, a thinning was produced after hardening using a milling cutter. The setting of a defined strength for the self-pierce riveting specimen was achieved by tempering the material afterwards. The welding tests were performed with press hardened material in different thicknesses to keep the influence of the AlSi-Coating during joining comparable. The 22MnB5 was used with sheet thicknesses of 1.0 mm, 1.5 mm and 2.0 mm. For each specimen, furnace parameters were selected that allowed a similar AlSi layer formation to minimise the influence of the coating on the welding lobe [24]. The specimens for resistance spot welding showed a hardness of over 490 HV1.

2.3.1. Resistance spot welding

For resistance spot welding, a material combination is used, which shows an insufficient connection of the outer sheet. A three-sheet stack-up consisted of two HX340LAD+Z100 sheets (1.5 mm, 0.7 mm) and one 22MnB5+AS150 (1.5 mm) sheet, as can be seen in Fig. 4. Resistance spot welding was performed, using the NIMAK Magnetic Drive C-type standalone welding machine, described in detail in [25] with a magnetic force control unit. Electrode tips from CuCr1Zr were used. Prior to the determination of the weldability lobe, they were milled to achieve the electrode geometry F1-16-20-50-6. Table 1 shows the welding parameters.

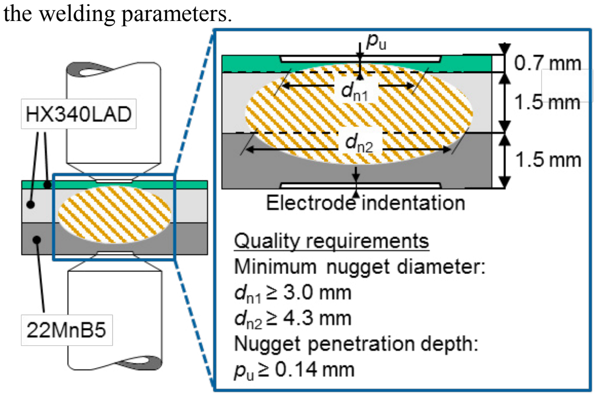

Fig. 4. A schematic depiction of a three-sheet stack-up with depicted joining plains, nugget penetration depth into the thin sheet p_u.

Table 1. Welding parameters according to SEP 1220-2 [26].

Squeeze time in ms	Welding time in ms	Holding time in ms	Electrode force in kN	Electrode shape DIN EN ISO 5821:2010-04
300	380	200	4.5	F1-16-20-50-6

To determine weldability lobes, a procedure, described in SEP 1220-2 was used [26]. Two welds were made per current setting. If at least one of them was expulsion-free, the welding current was increased by 0.2 kA and further two welds were made. This procedure was repeated until the current setting (I_u) was reached at which both produced welds had an expulsion. After that, welding current was decreased with the step of 0.1 kA until four subsequent expulsion-free welds could be produced with the same welding current. The welding current, at which the expulsion-free welds are possible, is referred to as I_{max} or the upper limit of the weldability lobe. The range above I_{max} is denoted as the unstable region. For the determination of the lower welding current (I_{min}), as a quality requirement, a minimum nugget diameter of d_n of 3.4 multiplied by square root of the sheet thickness must be approached. In addition, all welds must fulfil the quality requirements shown in Fig. 4. For specimens, welded with I_{min} and I_{max}, cross-sections were made, using the standard preparation procedure in compliance with DVS 2916-4 [27]. Nugget diameters in both joint plains and nugget penetration depth into the thin sheet were measured.

2.3.2. Self-pierce riveting

A Rivet Gen2 tool from Böllhoff with a maximum setting force of 78 kN was used for the self-pierce rivet investigations. The rivet types were special RIVSET® HDX rivets for hardened materials. After generating a local strength reduction, alternative rivet types (P, HD2, HD3) and dies are tested for their application. The selected material was a 22MnB5+AS150 (1.0 mm, 1.5 mm, 2.0 mm) and aluminium AA6016 (2.0 mm). Fig. 5 shows the required quality for the joining of self-pierce riveting in compliance with [11].

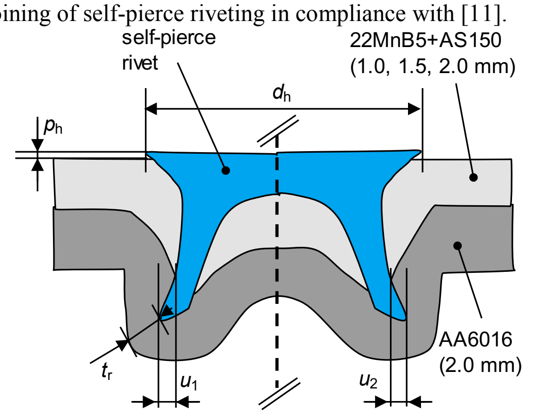

Explanation	Used quality requirements
d_h – head diameter p_h – rivet head position t_r – min. die side material thickness $u_{1,2}$ – undercut $u_{h1,2}$ – vertical undercut	Minimal undercut: $(u_1 + u_2)/2 \geq 0.1$ mm Minimal die side material thickness: $t_r \geq 0.05$ mm *No cracks*

Fig. 5. A schematic illustration of a self-pierce riveting with the quality requirements, according to DVS/EFB 3410 [11].

3. Results and Discussion

3.1. Demonstrator press hardening simulation

The experimentally recorded flow curves of the 22MnB5 sheet are shown in Fig. 6 for forming temperatures between 500 °C and 800 °C after heat treatment. The flow curves are used in the further numerical investigations.

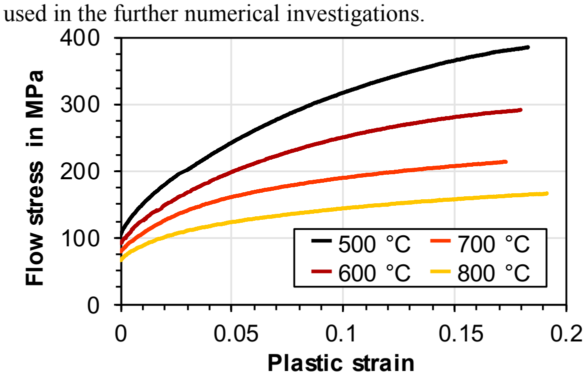

Fig. 6. Experimental flow curves for 22MnB5 after heat treatment.

The temperature distribution after the transfer from the furnace to the forming press is shown in Fig. 7 (a) for the sheet blank. After heating up to 930 °C, the sheet blank cools down to 729 °C in 7 s transfer time because of convection and thermal radiation. In Fig. 7 (b), the temperature distribution of the demonstrator after the hot deep drawing is presented. The lowest temperature is in the flange of the demonstrator and reaches values from 602 °C to 609 °C. Therefore, the creation of DIF is possible for any position of the local thinning in the flange.

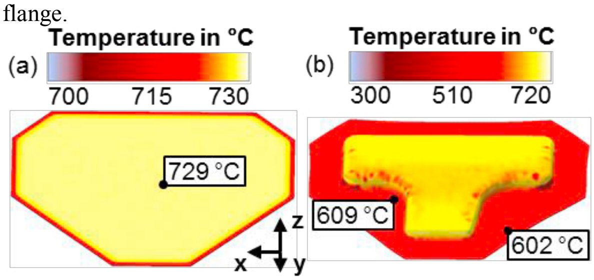

Fig. 7. Resulting temperature distribution after (a) transfer and (b) hot deep drawing.

Further, the distribution of the plastic strain after the hot deep drawing is analysed and depicted in Fig. 8 (a). The maximal plastic strain equals to 0.38 and is located at the radius of the punch. The plastic strain amounts from 0.02 to 0.04 in the flange. Therefore, the positions of the local thinning are located centrally in the flange as shown in Fig. 8 (b). The plastic strain after local thinning is 0.38 for the forming depth of 0.5 mm and evenly distributed over the sheet thickness. The forming force for creating one local thinning is 749 kN, and therefore two thinning can be experimentally created using a conventional forming machine. In addition, therefore the Weingarten impact bonding press type PSR 160 (forming force 2.500 kN) was chosen to perform the thinning experiments to ensure enough forming force. Further parameters like thinning punch diameter d_P, forming depth t_P and thinning punch edge radius r_P are investigated in [28].

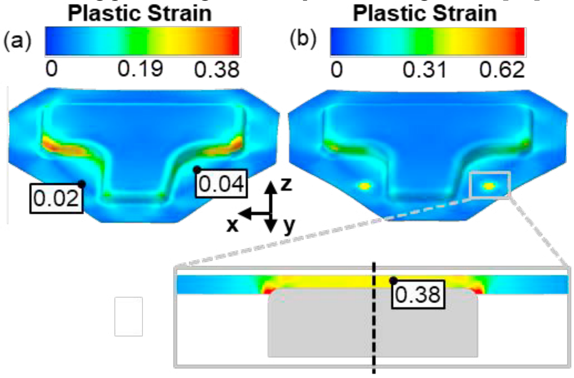

Fig. 8. Resulting plastic strain distribution after (a) hot deep drawing and (b) local thinning.

3.2. Local thinning and softening experiments

Forming experiments were carried out to produce a local thinning with reduced hardness of the sheet metal. The tests have shown that the heat treatment and the hardness of the tools, as well as the geometry of the deformation element, have a considerable influence on the thinning quality. It is determined that a high hardness of the tools is required to create a local deformation on the sheet metal. Various tools with different geometries of the deformation elements and hardness are used for this purpose. Fig. 9 shows the micro sections of the specimens created with different tools. The thinning in Fig. 9 (a) was produced with a convex tool surface.

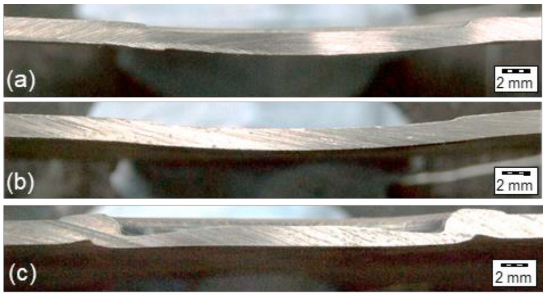

Fig. 9. Micrographs of the thinned specimen using (a) convex tool surfaces (initial hardness); (b) without convex die-side (54 HRC); (c) convex tool surfaces with maximum hardness.

The initial hardness of the tool surface was 48 HRC. It can be seen that no equal thinning took place. Due to the low hardness of the tool, the active surfaces are plastically deformed after a few forming tests. The tool used for the thinning in Fig. 9 (b) is not convex. For a better distribution of the forming forces, the tool was equipped with mechanical stops and hardened to a maximum of 54 HRC. The results of the deformation show, that the specimen does not achieve the desired geometry. Based on these results, a tool is developed which has a convex geometry on the die as well as on the embossed side and is hardened again to 54 HRC. The micro section, Fig. 9 (c), shows that the derived geometry of the thinning is only partially produced. The active surfaces of the tools used in the experiments are plastically deformed after a few strokes and could therefore not be further used. In order to get an optimal quality of the thinning with a plane thinning geometry a tool with hard metal (tungsten carbide) will be used in the future experiments. This should further prevent early tool failure so that a large number of specimen with reproducible thinning can be joined in the future work.

Nevertheless, more soft areas (311 HV1) could be produced in areas with higher deformation, i.e. in the edge area of the deformation element, while a martensitic structure (469 HV1) was found in the rest of the specimen. Fig. 10 depicts the edge area of a local thinning and softening.

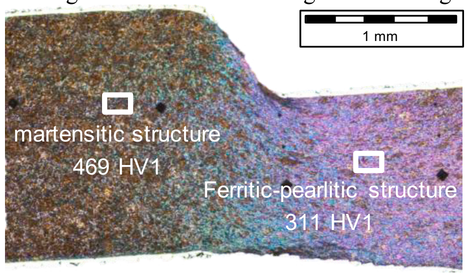

Fig. 10. Micro section of the edge area of a locally thinned and softened specimen with different hardness.

3.3. Joining of critical combinations

3.3.1. Resistance spot welding

As described in section 2.3, an analogy test was carried out to illustrate the effect of material thinning on resistance spot welding. Fig. 11 shows the effect of thinning by 0.5 mm on the weldability lobe and the nugget penetration depth into the thin sheet. Both together represent the process reliability.

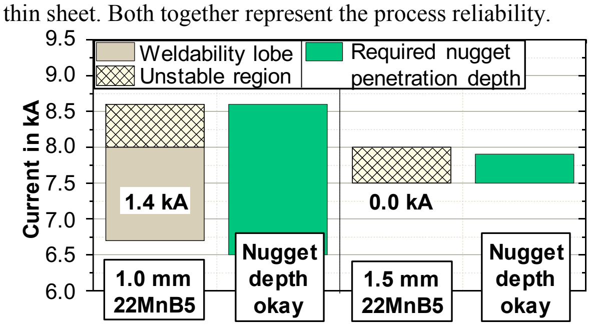

Fig. 11. Effect of 22MnB5 thinning on the weldability lobe and nugget penetration depth, equal welding parameters.

It can be deduced that with a reduction of the thickness, the welding lobe increases by 1.4 kA. To illustrate the influence of the sheet thickness, nugget cross-sections are prepared with respect to weld time of 90 ms, 185 ms and 380 ms at 7.5 kA weld current. As shown in the micro sections in Fig. 12, the initial formation of the welding nugget begins in the thinned 22MnB5 at a welding time of 90 ms. Also, a faster nugget growth in the direction of the middle sheet can be observed.

According to [29], the nugget grows first vertically and then horizontally. For this reason, it is essential to provide rapid initial nugget growth. More detailed investigations were carried out in [25]. At the end of the welding time, the thinned 22MnB5 stack-up has a larger nugget diameter and a higher penetration depth (HX340LAD/HX340LAD) than the not thinned stack-up.

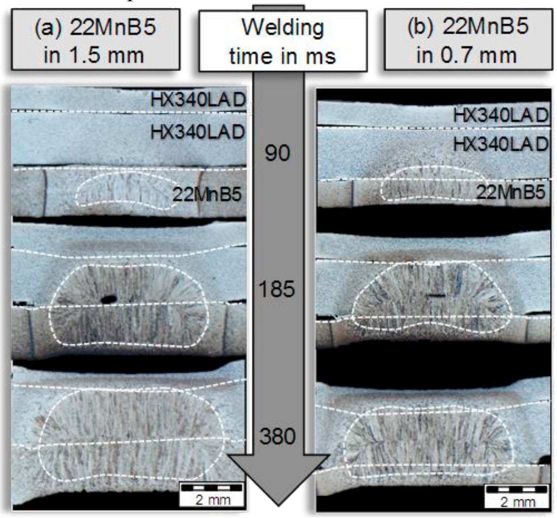

Fig. 12. Nugget cross-sections are showing nugget formation with respect to weld time of 90, 185 and 380 ms at 7.5 kA weld current: (a) 22MnB5+AS150 in 1.5 mm; (b) 22MnB5+AS150 in 0.7 mm

Press hardened sheets with locally milled thinning were produced to demonstrate the influence of local material reduction on the maximum shear tensile force. The specimens have the dimensions of 235 x 45 mm and a thinning with a diameter of 18 mm and a depth of 0.50 mm, as shown in Fig. 13.

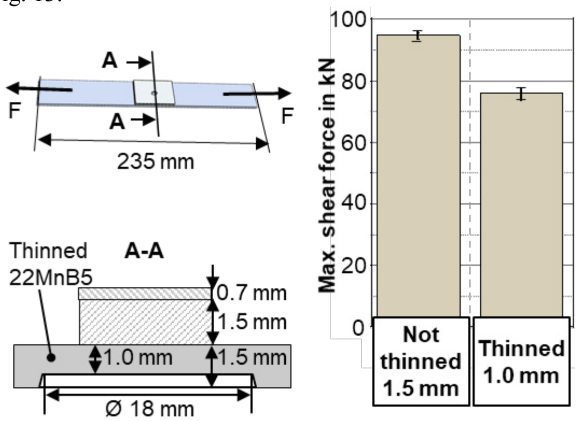

Fig. 13. Effect of local thinning in 22MnB5 on the maximal shear force.

The testing-machine used was a Zwick Roell Z250 and the test speed 10 mm/min. The local thinning causes a 19 % reduction in shear tensile force. Further investigations will be carried out to analyse the maximum achievable tensile force of thinned sheets with DIF.

3.3.2. Self-pierce riveting

For the joining investigations, the initial conditions, press hardened steels without local softening (i.e. over 490 HV1), were examined. Fig 14 shows the impact of the 22MnB5 thinning on the joinability, produced with special HDX rivets.

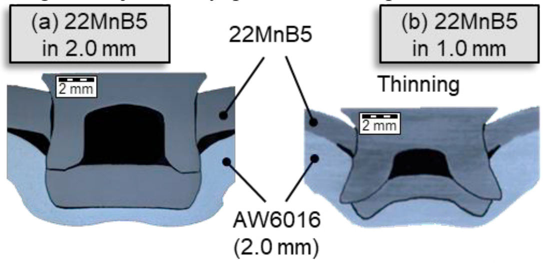

Parameters for punch riveting	
Hold-down force (binder)	2.0 kN
Setting force	60.0 kN
Type of rivet	**HDX** 6.5x5 H6
Die	SM 120 0130
Hardness (22MnB5)	> 490 HV1

Fig. 14. Effect of 22MnB5 thinning on the joinability produced with special HDX rivets.

The micro sections show that a suitable joint can only be produced if the 22MnB5 thickness is decreased from 2.0 mm. Even without microstructure modification, the process window of the self-pierce rivet can be enlarged by thinning the 22MnB5. In order to avoid the use of special HDX-rivets, it is necessary to change the local strength of the material. In the initial condition, i.e. with a sheet hardness of more than 490 HV1, the rivet types HD2 and HD3 cannot be joined as required [11]. In order to determine the hardness for a future DIF-thinning, milled samples were tempered at different temperatures. Fig. 15 shows an example of a thinned specimen with a hardness of 429 ± 5 HV1. It is possible to use the rivet types HD2 and HD3 with a sheet thickness of 1.0 mm to create an acceptable joint. The analogy test demonstrates that a thinning of the press hardened material reduces the hardness and therefore increases the process window for self-pierce riveting and resistance spot welding.

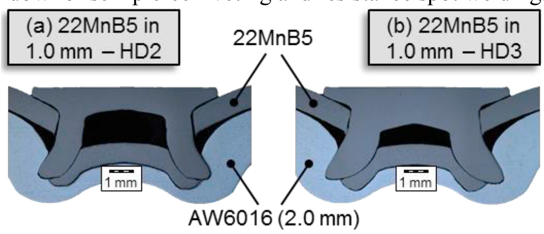

Parameters for punch riveting	
Hold-down force (binder)	6.0 kN
Setting force	55.0 kN
Type of rivet	**HD2** 5x5 H4
	HD3 5x5.5 H4
Die	SM 120 0208
Hardness (22MnB5)	429 ± 5 HV1

Fig. 15. Effect of 22MnB5 thinning on the joinability produced with (a) HD2 and (b) HD3 rivets.

4. Summary and Outlook

In this study, an extension of the conventional press hardening process is presented. Directly after hot deep drawing, a local deformation is introduced into the austenitic material to create deformation-induced ferrite (DIF). By deforming the material, a local thinning is achieved and the DIF in the deformed area results in a local softening. First, a press hardening process for a demonstrator is numerically modelled and used to investigate essential process parameters. It is estimated that two thinning punches can be integrated into the demonstrator tool. Second, an experimental setup was developed to perform local thinning and softening tests. Different tools are used to create a plane thinning point. First results show the creation of DIF and further tests have been performed to improve the quality of the thinning geometry. Further work is aimed at creating a sufficient quantity of specimen without tool failure. Finally, the initial condition without local deformation, as well as the influences of the local thinning and softening, were examined with analogy tests for resistance spot welding and self-pierce riveting. The results show an improved joinability for thinned and softened specimen. In future work, the punches for local thinning and softening will be integrated into the demonstrator tool. Press hardening tests with local thinning and softening in the flange will be carried out. Further joining investigations as well as analysis of the joint strength will be performed.

Acknowledgements

The authors gratefully acknowledge the financial support of the Research Association for Steel Application (FOSTA) and the German Federation of Industrial Research Associations (AiF) for this research work (AiF Ref.-No. 19797 BG). Furthermore, the authors would like to thank the industrial partners in this research project for the scientific exchange and discussion.

References

[1] Stockburger E, Wester H, Uhe J, Brunotte K, Behrens BA. Investigation of the forming limit behavior of martensitic chromium steels for hot sheet metal forming. Production at the leading edge of technology 2019:159-68.
[2] Behrens BA, Maier HJ, Nürnberger F, Schrödter J, Moritz J, Wolf L, Gaebel C. Hot forming and subsequent cooling outside the press for adjusted tailored properties of 22MnB5 steel sheets. Proceedings of 5th International Conference on Hot Sheet Metal Forming of High Performance Steel 2015:35-42.
[3] Meyer S, Meschut G, Vogt H, Neumann A, Hübner S, Behrens BA. Application of self-piercing nuts during hot forming of 22MnB5. Welding in the World 2019;63(15):1-10.
[4] Berjoza D, Jurgena I. Influence of batteries weight on electric automobile performance. Proceedings of 16th International Scientific Conference Engineering for Rural Development 2017:1388-94.
[5] Lian Y, Zeng D, Ye S, Zhao B, Wei H. High-Voltage Safety Improvement Design for Electric Vehicle in Rear Impact. Automotive Innovation 2018: 211-25.
[6] Deutscher Verband für Schweißen. Organisation und Schwerpunktthemen der Abteilung „Forschung und Technik“ im DVS. DVS-Technikreport 2017.
[7] Beckert M. Grundlagen der Schweisstechnik. Schweissverfahren. Verl. Technik 1993.
[8] Hwang IS, Kang MJ, Kim DC. Expulsion Reduction in Resistance Spot Welding by Controlling of welding Current Waveform. Procedia Engineering 2011;10:2775-81.
[9] Oi K, Murayama M. Recent trend of welding technology development and applications. JFE Tech. Rep 2015;20:1-7.
[10] Rudolf H, Rose S. Methoden zur Schweißlinsenverschiebung bei Mehrblechbverbindungen. 21. DVS-Sondertagung Widerstands-schweißen 2010:30-7.
[11] Deutscher Verband für Schweißen / Europäische Forschungs-gesellschaft für Blechverarbeitung e. V. Merkblatt DVS/EFB 3410 Stanznieten 2019.
[12] Kotschote C, Freudenberg P. Einsatz von Verbindung höchstfester Stählen im Multi-Material-Mix der Audi ultra–Leichtbaukarosserie. Proceedings of 10. Erlanger Workshop Warmblechumformung 2015:133-50.
[13] Behrens BA, Hübner S, Chugreev A, Bohne F, Seel A, Jalanesh M, Wölki K. Finite Element Analysis of the Phase Transformation during a Hot Stamping Process. Proceedings of 18th IFHTSE Congress 2010:4710-21.
[14] Banik J, Lenze FJ, Sikora S, Laurenz R. Tailored properties – a pivotal question for hot forming. Proceedings of Hot Sheet Metal Forming of High-Performance Steel 2011:20-33.
[15] Landgrebe D, Silbermann K, Pierschel N. Verfahren zur punktförmigen Bauteilgradierung beim Presshärten im Werkzeug. EFB-Forschungsbericht 2018;486.
[16] Zimmermann F, Spörer J. Partial tempering of press hardened steels by direct flame impingement. Proceedings of Hot Sheet Metal Forming of High-Performance Steel 2015:17-24.
[17] Schaefer M, Schuoecker D. Laser softening of press hardened steel in high volume production lines. Proceedings of Hot Sheet Metal Forming of High-Performance Steel 2015:25-33.
[18] Meschut G, Matzke M. Lokale Konditionierung von presshartem Vergütungsstahl für das Hybridfügen von Mischbaustrukturen. Proceedings of 13. Kolloquium Gemeinsame Forschung in der Klebtechnik 2013:33-42.
[19] Drillet P, Grigorieva R. Study of cracks propagation inside the steel on press hardened steel zinc based coatings. Metallurgia Italiana 2012;1:1-8.
[20] Dong H, Sun X. Deformation induced ferrite transformation in low carbon steels. Current Opinion in Solid State and Materials Science 2005;9:269-76.
[21] Min J, Lin J. On the ferrite and bainite transformation in isothermally deformed 22MnB5 steels. Materials Science and Engineering A 2012;550:375-87.
[22] Somani MC, Karjalainen LP. Dimensional changes and microstructural evolution in a B-bearing steel in the simulated forming and quenching process. ISIJ International 2001;41:361-7.
[23] Olle P, Voges-Schweiger k, Behrens BA. Finite Element Analysis of the Phase Transformation during a Hot Stamping Process. Proceedings of 18th IFHTSE Congress 2010:4710-21.
[24] Sherepenko O, Luo Y, Schreiber V, Wohner M, Mitzschke N, Kuhlmann M, Jüttner S. Influence of Press-Hardening-Process on Resistance Spot Weldability of 22MnB5+AS150 with Aluminium-Silicon Coating in a Three-Sheet Stack-Up for Automobive Applications. Proceedings of 7th International Conference Hot Sheet Metal 2019:395-402.
[25] Wohner M, Mitzschke N, Ullrich M, Jüttner S. Optimierung des Widerstandspunktschweißens auf Basis einer Prozessdatenanalyse. 14 Magdeburger Maschinenbau-Tage 2019:269-79.
[26] SEP 1220-2:2011-08 - Testing and Documentation Guideline for the Joinability of thin sheet of steel 2011.
[27] Deutscher Verband für Schweißen. Merkblatt DVS 2916-4 - Prüfen von Widerstandspressschweißverbindungen 2006.
[28] Stockburger E, Müller F, Chugreev A, Behrens BA. Advanced FE-simulation of press-hardening regarding joining ability and tool hardness estimation. Proceedings of Forming Technology Forum 2019:1-8.
[29] Iyota M, Mikami Y. Numerical Simulation of Nugget Size and Residual Stress of Resistance Spot Welded HT 980 Steel Sheet. Quarterly Journal of the Japan Welding Society 2011;29(2):86-95.